Received 29 August 2025 | Revised 15 November 2025 | Accepted 09 December 2025
Vol. 06, No. 02, page 142-154

RESEARCH ARTICLE TUJES Tobruk University Journal of Engineering Sciences

Effect of Bundled GFRP Bars on Thermal Cracking Behavior

O. R. ELzaroug[1], J. P. Forth[2], J. Q. YE[3]

[1]Department of Civil Engineering, Omar El-Mukhtar University
[2]School of Civil Engineering, University of Leeds
[3]Department of Engineering, Lancaster University
omerelzaroug@yahoo.com

Abstract. The mismatch in thermal expansion between Glass Fiber Reinforced Polymer (GFRP) bars and concrete generates internal stresses as temperature increases. These stresses may lead to splitting cracks around the reinforcement, weakening the bond, reducing structural capacity, and increasing deflection. This study investigates, both experimentally and numerically, the effects of transverse thermal incompatibility between GFRP and concrete on the behavior of GFRP-reinforced concrete slabs subjected to a linear temperature rise from 20°C to 100°C. A nonlinear finite element (NLFE) analysis using DIANA software [1] was conducted to determine the temperature at which the first transverse crack initiates at the bar surface, the corresponding tensile stress. The model was also used to predict the extent and pattern of thermally induced cracking caused by the thermal mismatch between concrete and GFRP bars. Verification of the NLFE model was performed by comparing the results of the proposed 2D simulation with experimental findings. The results confirmed the significant effect of temperature variations on the stress state within GFRP-reinforced concrete slabs and highlighted the need for a minimum concrete cover to prevent crack propagation through the slab. Overall, the NLFE model showed good agreement with the experimental results for a concrete cover equal to 1.5 to 2, times the bar diameter.

Keywords: GFRP, thermal cracking, nonlinear analysis, concrete, bond.

1. Introduction

The use of non-metallic fiber-reinforced polymer (FRP) reinforcement as an alternative to steel in concrete is increasingly accepted due to its superior corrosion resistance. Its high strength-to-weight and stiffness-to-weight ratios, along with ease of handling, further enhance its appeal. However, a clearer understanding of the thermal behavior of FRP-reinforced concrete under significant temperature variations remains essential for ensuring reliable structural performance.

Glass FRP bars exhibit orthotropic thermal expansion properties, with a transverse coefficient of thermal expansion (CTE) that is 5 to 8 times higher than that of concrete [2, 3]. This thermal mismatch generates radial pressure at the interface between the GFRP bar and the surrounding

concrete as temperature rises, leading to tensile stresses within the concrete. If these stresses exceed the concrete's tensile capacity, cracking may occur and significantly weaken the FRP–concrete bond [4]. Such thermally induced stresses can also cause transverse cracking in the concrete (Fig. 1) [5, 6], reducing both serviceability and long-term durability of the structure [7]. In severe cases, insufficient confinement may lead to spalling of the concrete cover [6, 8, 9].

Figure 1 Thermal cracking due to transverse expansion of GFRP [5]

Gentry and Husain [10] developed an analytical model to examine the tensile stresses generated in the concrete surrounding an FRP bar under a uniform temperature increase of 40°C. The model assumes that the FRP bar is transversely isotropic and incorporates the effect of the bar's longitudinal strain resulting from mechanical loading. This analytical approach is valid only for FRP bars without helical wrapping and for temperature changes up to 40°C.

Rahman *et al*. [11] analyzed the hoop stresses responsible for radial cracking by modeling a concrete ring surrounding the FRP reinforcement. As temperature increases, the significant transverse expansion of the FRP bar generates a radial pressure on the surrounding concrete, leading to the development of these stresses.

Bellakehal and Zaidi [12] developed an analytical model to examine the effect of transverse thermal expansion on vertically overlapped FRP bars embedded in prismatic concrete beams. To simplify the analysis, they proposed replacing the two bars with a single equivalent bar when calculating the critical and service temperature changes using the established equations.

Gentry and Husain [13] investigated the thermal compatibility of E-glass/vinylester FRP rebars with smooth and helical surfaces, in diameters of 12 mm and 20 mm, embedded in concrete with covers of 10–50 mm and a compressive strength of 30 MPa. The specimens were subjected to a 40°C temperature rise, and nonlinear thermoelastic simulations using COSMOS-M assessed concrete cracking. Results showed that smaller bar diameters and higher concrete confinement reduced the incidence of cracking.

Abdalla [14] investigated the effect of concrete cover on FRP-reinforced concrete under elevated temperatures using analytical, numerical, and experimental approaches. Nonlinear numerical analysis of rectangular elements with 16-mm FRP bars and concrete covers of 20 mm and 30 mm, exposed to temperature changes up to 50°C, showed that maximum tensile stresses

at the bar–concrete interface were lower than analytical predictions by 11% for a small cover-to-bar-diameter ratio and 14% for a larger ratio highlighting the influence of concrete cover on stress reduction.

El-Zaroug *et al*. [15] used 2D nonlinear finite element analysis to study thermal mismatch between concrete and GFRP bars with temperatures from 20°C to 100°C. Results showed that differences in transverse expansion cause variable stress patterns. To limit cracking at temperatures up to 60°C, they recommended vertical cover >1.5 times bar diameter, horizontal cover ≥50 mm, smaller bars, and stronger concrete. The simulations agreed well with experiments for a 1.5db cover.

Zaidi *et al*. [16] used finite element analysis on concrete cylinders with FRP bars to study the effect of the bars' transverse elastic modulus under rising temperatures. Concrete was modeled with tensile softening, and FRP bars as linear elastic and brittle. Results showed higher stresses with increased FRP transverse modulus, while concrete cover thickness had little effect on strain. To reduce splitting in hot environments, a cover-to-bar ratio of at least 2 was recommended, with splitting stresses increasing for higher cover ratios and stronger concrete.

Lardjane *et al*. [17] used ADINA to simulate the thermal behavior of concrete slabs reinforced with GFRP bars, examining cover-to-bar ratios from 1.3 to 2.8 and temperatures from -50°C to 60°C. Initial cracking occurred between 15°C and 30°C, depending on the cover ratio and concrete tensile strength. No splitting was observed at negative temperatures, while cover splitting occurred between 30°C and 59°C, with a typical case at 46°C. Finite element results closely matched analytical predictions and experimental data for stresses, strains, and cracking temperatures.

Yi [18] studied the effect of transverse thermal expansion of FRP bars on concrete cover using theoretical and 2D nonlinear Abaqus simulations on cylinders with varying bar diameters and cover thicknesses, over temperatures from -70°C to 80°C. Results showed that FRP-reinforced concrete behaves elastically up to a 20°C temperature change; beyond this, cracking develops and inelastic behavior occurs. Negative temperature changes caused compression, closely matching theoretical strains, while positive changes induced tensile stresses and cracks, with FEM results 1.2–1.4 times higher than theoretical values. Concrete cover thickness significantly influenced cracking, and the FEM approach effectively captured inelastic behavior.

Saleem and El-Zaroug [19] conducted a finite element analysis using DIANA to predict thermal loads causing initial cracks and concrete cover splitting in GFRP-reinforced slabs under temperature rises up to 80°C. They considered cover thickness, bar diameter, bar spacing, and concrete grade. Results showed that cover thickness, bar diameter, and concrete strength affect the onset of cracking and cover splitting, while bar spacing significantly influences crack patterns.

A 2D nonlinear finite element (NLFE) analysis was used to capture effects not addressed by previous analytical models. Unlike linear-elastic models, NLFE accounts for stress redistribution after concrete cracking and more accurately predicts cracking at the FRP–concrete interface, including crack initiation and propagation. It also accommodates variable concrete cover

thickness and incorporates temperature–time effects on material properties, which analytical models could not consider.

2. Material Properties

2.1 GFRP Bras

Type E GFRP bars (Fig. 2 [20]) were used, made of continuous E-glass fibers (70% by volume) in a vinyl-ester resin matrix with a sand-coated, wrapped surface to improve bond and reduce transverse thermal expansion. The bars had a longitudinal modulus of 40.8 GPa, ultimate strengths of 690MPa for 13 mm diameters, and thermal expansion coefficients $\alpha_L = 6.58\times10^{-6}$/°C and $\alpha_T = 33.7\times10^{-6}$/°C. The stress–strain behavior of GFRP bars is linear until failure (Fig. 3). GFRP consists of glass fibers embedded in a vinyl-ester resin matrix, making it less resistant to high temperatures than steel. Mechanical properties degrade near or above the glass transition temperature (T_g), reducing stress transfer between concrete and fibers. For GFRP, T_g = 115°C [21]. Specimens with 13 mm diameter exposed to 100°C showed no visible damage, and tensile capacity remained largely unaffected, as this temperature is below the T_g.

Figure 2 GFRP bars

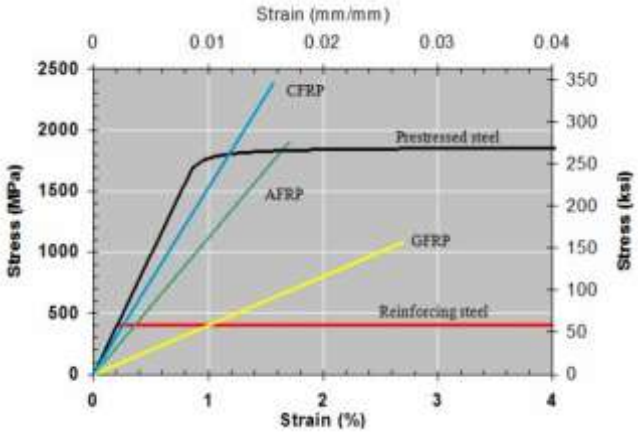

Figure 3 Stress-strain for different materials

2.2 Concrete

The concrete mix had a water–cement ratio of 0.55**,** consisting of 355 kg/m³ Portland cement**,** 195 kg/m³ water**,** 724 kg/m³ fine aggregate, and 1086 kg/m³ coarse aggregate (maximum 20 mm). No superplasticizer was used. The concrete achieved an average cube compressive strength of 50 MPa and an average splitting tensile strength of 3.2 MPa**.**

3. Experimental Program

Five concrete slabs were cast and tested with identical dimensions of 500 × 150 mm and a length of 2800 mm. Longitudinal reinforcement consisted of single GFRP bars (13, 16, 19 mm) and bundled bars (13 and 16 mm) without stirrups. The variables investigated were the

reinforcement ratio (ρ_f), bar diameter (d_b), clear bar spacing (cbs), and concrete cover (c), and all slabs were heated to 100°C. Reinforcement details are summarized in Table 1.

Each slab was simply supported and exposed to thermal loading only. As shown in Figure 4, the heat was applied to the bottom surface using nine infrared bulbs (250 W each), producing a temperature gradient up to 100°C. The heating system consisted of an insulated wooden box, sized 500 × 500 × 2000 mm, constructed from 18 mm plywood and lined internally with aluminum foil, with an additional 7 mm Rockwool layer applied externally to reduce heat loss. This box was fixed to the underside of the slab over a 2000 mm length, while all other faces of the specimen were insulated to ensure effective heat transfer through the bottom surface only.

Table 1 Details of test Specimens

Slab specimens	No. of bars	d_b (mm)	ρ_f (%)	c (mm)	cbs (mm)	GFRP arrangement	Treatment
SG13-4-1	4	12.70	0.82	20	116	Single bar	Heated up to 100°C
SG16-3-1	3	15.88	1.02	25	176		
Sg19-4-1	4	19.05	2.07	30	108		
SG13-6-2	6	12.70	1.23	20	162	Two bundled bars	
SG16-6-2	6	15.88	2.03	25	152		

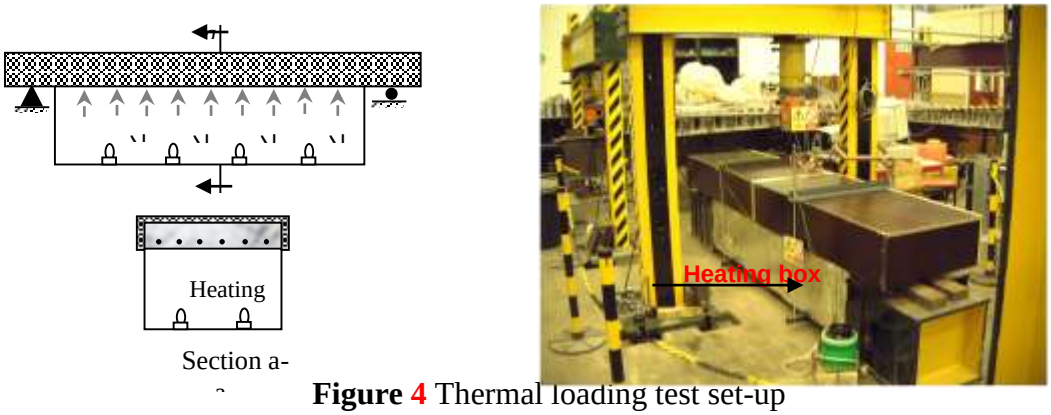

Section a-

Figure 4 Thermal loading test set-up

Temperature distribution through the slab depth was recorded using seven thermocouples embedded in the concrete. At two positions along the heated zone, spaced 667 mm apart, two thermocouples were installed horizontally and vertically with 50 mm depth spacing at each location. A fifth thermocouple was fixed directly to a GFRP bar, while the remaining two were placed externally on the heated (hot) surface and the unheated (cool) surface. This configuration allowed accurate evaluation of the temperature gradient through the slab thickness and ensured verification of temperature uniformity along the heated region.

Two types of strain gauges were used on the GFRP rebars: 5 mm gauges for longitudinal strain and 2 mm gauges for transverse strain [21]. Each rebar carried two transverse and one longitudinal gauge within the 2000 mm heated zone to monitor thermal deformation. All slabs were simply

supported, with one end on a roller to allow expansion and the other on a hinge, maintaining a 2400 mm span (Fig. 2).

4. Testing Procedure

Specimens underwent a single thermal cycle on the tension side, with temperature raised in 15°C increments to 100°C and held to stabilize, followed by cooling. The cycle lasted approximately 15 hours. The test assessed GFRP transverse thermal movement, cracking, and bond behavior. Responses were monitored using thermocouples, strain gauges, and LVDTs, with measurements every 20 minutes, and the hot surface checked for cracks.

5. Description of 2D NLFE Model

Thermally induced cracking mainly developed in the lateral (cross-section) direction, leading to bond loss between the GFRP bar and the surrounding concrete; therefore, longitudinal thermal stresses were neglected. A 2D NLFE model (Fig. 5) was adopted to simulate concrete cracking, occurring when the thermal stress around the GFRP bar locally reached the concrete tensile strength.

For simplification, the slab cross-section was modeled with a single GFRP bar (diameters: 13 mm) to predict radial cracks under temperature rise. The model dimensions were based on the tested specimens: total width = 100 mm concrete cover (2×50 mm) plus bar diameter (d_b), and height = 0.5d_b + concrete cover.

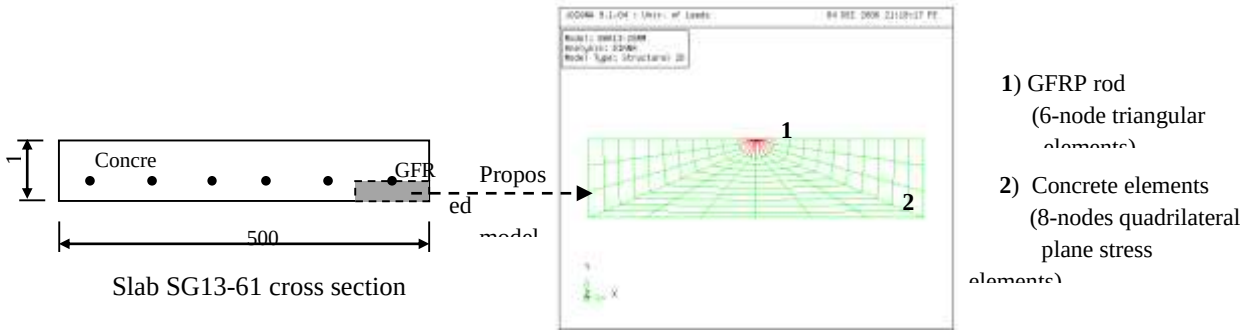

Figure 5 NLFE model of GFRP rod embedded in concrete

6. Analysis Process for NLFE Model

The nonlinear FE analysis used a linear stress cut-off criterion, where cracking initiated once the principal tensile stress exceeded the concrete tensile strength. Concrete tension was modeled as brittle, and compression followed Von Mises ideal plasticity. Temperature-dependent material behavior was defined through a time-based input table, and the analysis was run in time steps using EXECUT commands.

Heating was applied gradually in 1°C increments up to 80°C, while larger increments were used during cooling to reduce computation time without affecting results. Convergence was based on displacement with a tolerance of 0.01. All steps converged, though iteration counts varied. The Regular Newton-Raphson method was used for stiffness updates and nonlinear response, with a limit of 100 iterations.

7. Results Presentation

A nonlinear numerical analysis was conducted to determine the temperature levels associated with maximum tensile stress (ΔT_t), first transverse crack initiation (ΔT_{cr}), and concrete cover splitting (ΔT_{sp}). The numerical findings were compared with experimental results from full-size slabs, with emphasis on thermal stress development and thermally induced cracking. Five NLFE models, representing slabs reinforced with single, double, and triple bundled GFRP bars, were analyzed and designated as Model 1to 5 according to Table 2.

7.1 Thermal Stresses in Concrete Section

Figures 6 and 7 present the nonlinear FE results of the principal thermal stresses in the GFRP bars and the surrounding concrete just before the initiation of first cracking due to temperature rise in the slab cross-section. The analysis included both single and two bundled GFRP bars (Table 1). A concrete cover of $1.5d_b$ was adopted for all bar sizes.

Table 2 Cracking temperatures in Diana models

Models	Slab specimens	f_c (MPa)	f_{ct} (MPa)	d_b (mm)	c (mm)	α_t ($^oC^{-1}$)	c/d_b (mm)	ΔT_{cr} (^{o}C)	ΔT_{sp} (^{o}C)
								DIANA	
M1	SG13-4-1	46	2.8	12.70	20	$23x10^{-6}$		51	-
M2	SG16-3-1	49	3.1	15.88	25	$25x10^{-6}$		47	65
M3	Sg19-4-1	53	3.3	19.05	30	$27x10^{-6}$	1.5	44	
M4	SG13-6-2	55	3.5	12.70	20	$23x10^{-6}$		42	-
M5	SG16-6-2	47	3.2	15.88	25	$25x10^{-6}$		32	80

- ΔTsp not observed in DIANA simulations.

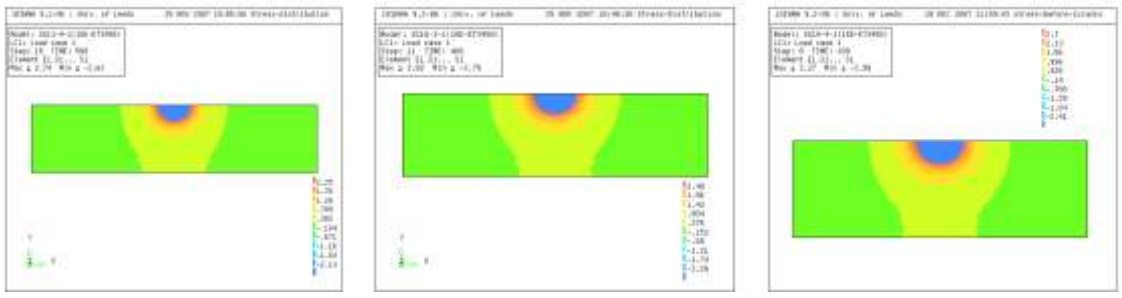

ΔT$_t$ = 50°C
a) M1 (13 mm)

46°C
b) M2 (16 mm)

43°C
c) M3 (19 mm)

Figure 6 Stress distributions just before initial crack

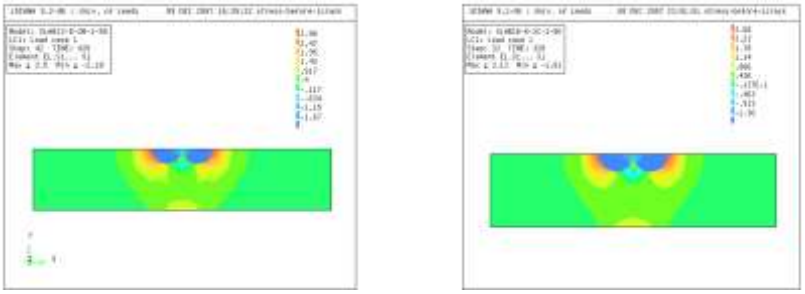

ΔT_t = 41ºC 31ºC

a) M4 (13 mm) b) M5 (16 mm)

Figure 7 Stress distributions just before initial crack

Thermal stresses in M1 (13 mm) developed at a temperature change (ΔT_t) of 50 °C (Fig. 6a), while the corresponding ΔT_t decreased for the larger bar in M2 (16 mm) and M3 (19 mm) (Fig. 6 b & C). It was also observed that ΔT_t decreased from 50 to 41 °C and from 46 to 31 °C when using two bundled GFRP bars for the 13 mm and 16 mm cases, respectively, due to the larger interface area between the GFRP and concrete. These stresses, present both within the concrete and at the GFRP/concrete interface, result from the mismatch between the transverse thermal expansion coefficients of the GFRP and concrete. In the DIANA simulations, the tensile stress in the concrete propagated outward from the GFRP/concrete interface and gradually diminished toward the outer fibers of the section, independent of the concrete cover. Although relatively small, compressive stresses developed at the corners of the section (Figs. 6 and 7).

7.2 Cracking Behaviour

7.2.1 Initial Cracking

Figure 8 shows the predicted distribution of initial cracks in slabs reinforced with single GFRP bars (13, 16, and 19 mm) and two bundled bars (13 and 16 mm), with a concrete cover of c = $1.5d_b$ at various elevated temperatures. Crack initiation occurred at the interface surrounding the GFRP bars at different temperature levels. This behavior resulted from the mismatch in the transverse thermal expansion between the GFRP bars and the concrete, which generated radial stresses, reduced bond, and led to crack formation.

Among the single-bar specimens, the earliest crack initiation was observed in Model M3, reinforced with a 19 mm bar (Fig. 8c), due to its larger perimeter and greater transverse expansion (see Table 2). In contrast, models with two bundled bars developed initial cracking at even lower temperatures, with the lowest temperature value recorded in Model M5 at 32°C.

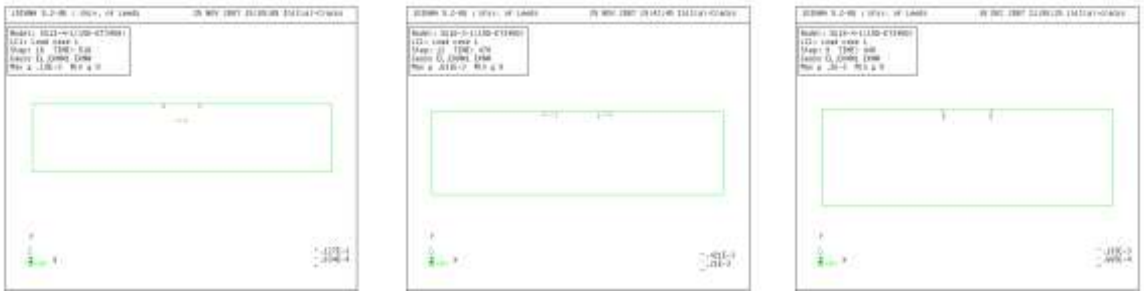

ΔT_t = 51°C
a) M1 (13 mm)

47°C
b) M2 (16 mm)

44°C
c) M2 (16 mm)

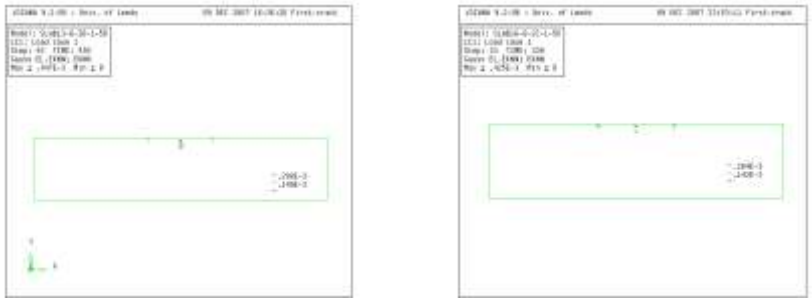

42°C
c) M4 (13 mm)

32°C
d) M5 (16 mm)

Figure 8 Initial cracking patterns

7.2.2 Cracking at ΔT_t = 80°C

Figure 9 illustrates the cracking behavior of the models with a constant cover-to-diameter ratio of c/d_b = 1.5 (Table 2) under a maximum temperature rise of ΔT_t = 80°C. Following crack initiation, crack length gradually increased as temperature continued to rise. In models M1 and M2 (single GFRP bars), cracks formed around the bar and progressed through the concrete cover without reaching the outer faces of the specimens (Fig. 9 a & b).

In contrast, Model M3 provided with 19 mm GFRP exhibited more extensive crack growth; several cracks propagated further and eventually reached both sides of the section (Fig. 9c). Notably, major cracks did not reach the edges until the temperature exceeded 65°C. Thermal deterioration in M3 initiated around the bar, penetrated the concrete cover, and ultimately resulted in splitting failure. The observed splitting closely resembled the failure pattern recorded in the corresponding heated slab specimen (Fig. 10a).

Models M4 and M5, reinforced with bundled GFRP bars of 13 mm and 16 mm, showed cracks forming around the bars and propagating through the concrete cover without reaching the outer faces (Fig. 9 d & e). In Model M5, cracks also appeared at the bottom surface (Fig. 9e), similar to the experimental pattern of slab SG16-6-2 (Fig. 10b), aligned with the longitudinal bars. The bottom cracking in M5 is attributed to the larger bond area of the bundled bars and the mismatch in transverse thermal expansion, which caused high transverse movements and tensile stresses around the bars.

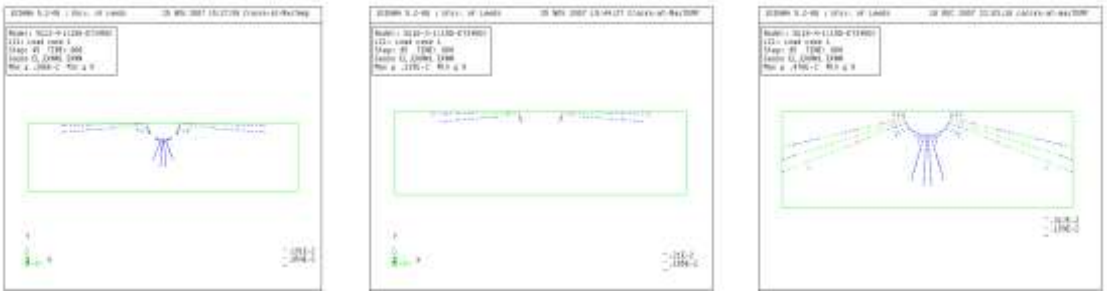

a) M1 (13 mm) b) M2 (16 mm) c) M2 (19 mm)

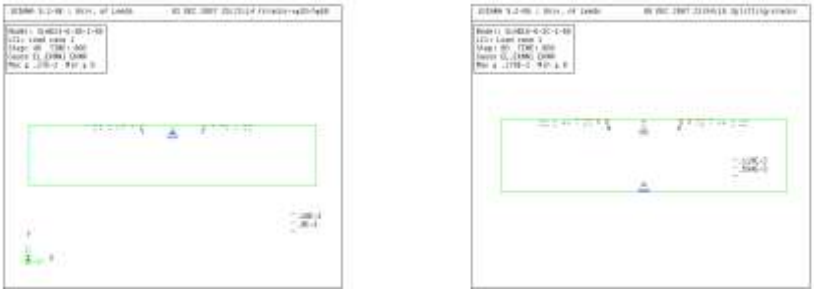

d) M4 (13 mm) e) M5 (16 mm)

Figure 9 Cracking patterns due to ΔT_t of 80°C

The DIANA analysis revealed that increasing the cover-to-bar ratio (c/d_b) effectively reduced the length of thermally-induced cracks. Specifically, in Model M4, raising c/d_b from 1.5 to 2.5 shortened the cracks (Fig. 11), while in Model M5, an increase from 1.5 to 2 led to a noticeable reduction in crack length (Fig. 12). This adjustment also decreased the associated thermal crack strains.

For Model M4, no significant change in crack length was observed when c/d_b increased from 1.5 to 2, whereas a further increase to 2.5 produced a clear reduction. Additionally, the crack strain at c/d_b = 2.5 was lower than the strains measured at c/d_b values of 1.5 and 2, indicating improved thermal performance with thicker concrete cover.

a) M3 (19 mm) b) M5 (16 mm)

Figure 10 Experimental Cracks observed on slabs SG19-4-1 & SG16-6-2

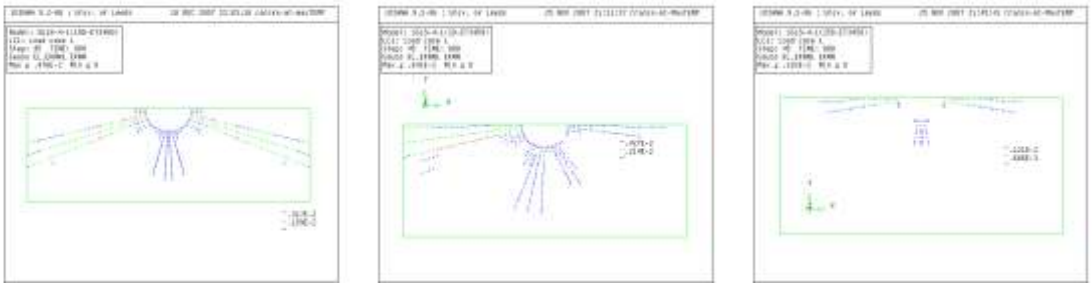

a) c/d_b = 1.5 b) c/d_b = 2 c) c/d_b = 2.5

Figure 11 Cracking Patterns of NLFE M4 due to 80°C

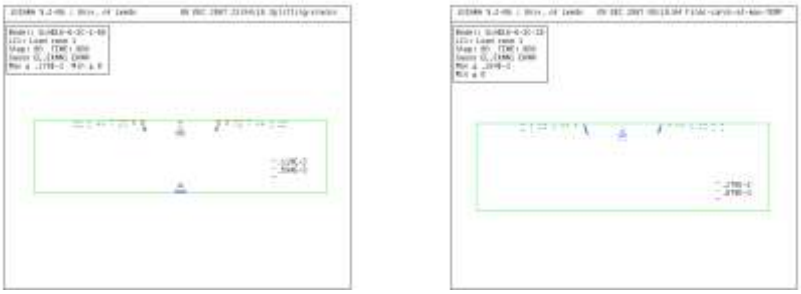

a) c/d_b = 1.5 b) c/d_b = 2

Figure 12 Cracking Patterns of NLFE M5 due to 80°C

The NLFE simulation offers a distinct advantage in its ability to predict both thermal stress distribution and the progression of cracking. Unlike analytical methods, it can capture the development and spread of cracks, which cannot be reliably represented through analytical modelling alone.

8. CONCLUSIONS

The NLFE simulations demonstrated that thermal incompatibility between concrete and GFRP reinforcement leads to stress variation and transverse cracking, which intensifies with increasing bar diameter and becomes more critical when using bundled bars. Conversely, higher concrete strength and adequate confinement effectively reduce crack initiation and propagation. To limit thermally induced cracking at temperatures up to 80 °C, the results recommend a minimum vertical cover of $\geq 1.5\ d_b$ for single small bars and $\geq 2.5\ d_b$ for larger bundled bars, in addition to a horizontal cover of $\geq$ 50 mm. The study further indicates that using smaller bar diameters enhances the thermal performance and mitigates stress concentration at the concrete–bar interface. Numerical predictions showed close agreement with experimental findings at 1.5 d_b, confirming the reliability of the adopted NLFE model.

9. Reference

1. DIANA Finite Element Analysis (2005). User's Manual Release 9. TNO DIANA BV. Delft, the Netherlands.
2. Matthys, S., De Schutter, G. and Taerwe, L. (1996). Influence of transverse thermal expansion of FRP reinforcement on the critical concrete cover. *In: the second international conference on advanced composite materials in bridges and structures*. Montreal, Canada, August 1996, pp. 665-672.
3. Challal, O. and Benmokrane, B. (1993). Physical and mechanical performance of an innovative glass fiber reinforced plastic rod for concrete and grouted anchorages. *Canadian Journal of Civil Engineering*, 20 (2), pp. 254-268.
4. Rahman, A.H., Kingsley, C.Y. and Taylor, D.A. (1995). Thermal stress in FRP-reinforced concrete. *In: annual conference of the Canadian society for Civil Engineering.* Ottawa, Canada, 1-3 June 1995, pp. 605-614.
5. Abdalla, H.A. and Elbadry, M.M. (1997). Temperature effects on concrete members reinforced with FRP reinforcement. *In: the 25th annual conference of the Canadian society for civil engineering*. Sherbrooke, Canada, May 1997, pp. 171-180.
6. EL-Zaroug, O. R., Forth, J. P., YE, J. Q. and Beeby, A. W. (2007). Flexural performance of concrete slabs reinforced with GFRP and subjected to different thermal histories. *In*: *the 8th international symposium on Fiber-reinforcement polymer reinforcement for concrete structures (FRPRCS-8).* Patras, Greece, July 16-18, 2007, pp. 1-10.
7. Elbadry, M.M. and Abdalla, H.A. (1998). Experimental studies on thermal cracking in concrete member reinforced with FRP. *In: the first conference on durability of fiber reinforced polymer (FRP) composites for construction*, CDCC98. Sherbrooke, Canada, August 1998, pp 669-680.
8. Aiello, M.A., Focacci, F., Huang, P.C. and Nanni, A. (1999). Cracking of concrete cover in FRP reinforced concrete elements under thermal loads. *In*: *the 4th international symposium on FRP for reinforcement of concrete structures (FRPRCS4).* Baltimore, MD, November 1999, pp. 233-243.
9. Elbadry, M.M., Abdalla, H. and Ghali, A. (2000). Effects of temperature on the behaviour of fiber reinforced polymer reinforced concrete members. *Canadian Journal of Civil Engineering*, 27, pp. 993-1004.
10. Gentry, T.R. and Husain, M. (1999). Thermal compatibility of concrete and composite reinforcement. *Journal of Composites for construction,* 3 (2), pp. 82-86.
11. Rahman, A.H., Kingsley, C.Y. and Taylor, D.A. (1995). Thermal stress in FRP-reinforced concrete. *In: annual conference of the Canadian society for Civil Engineering.* Ottawa, Canada, 1-3 June 1995, pp. 605-614.
12. Bellakehal, H., & Zaidi, A. (2016). Analytical model of overlapped FRP bars embedded in Concrete under high temperature. 5. https://doi.org/10.15224/978-1-63248-096-5-17.
13. Gentry, T. R., & Husain, M. (1999). Thermal Compatibility of Concrete and Composite Reinforcements. Journal of Composites for Construction, 3(2), 82–86.
14. Abdalla, H. (2006). Concrete cover requirements for FRP reinforced members in hot climates. Composite Structures, 73(1), 61–69.
15. EL-Zaroug, O., Forth, J., & Ye, J. (2013). Prediction of thermal cracking in concrete structures reinforced with GFRP (J. Barros, Ed.). Elsevier.
16. Zaidi, A., Brahim, M. M., Mouattah, K., & Masmoudi, R. (2017). FRP Properties Effect on Numerical Deformations in FRP Bars-Reinforced Concrete Elements in Hot Zone. Energy Procedia, 139, 798–803.
17. Lardjane, S., Bellakehal, H., Zaidi, A., & Masmoudi, R. (2018). Numerical simulation of one-way concrete slabs reinforced with glass fiber reinforced polymer bars under service temperatures. Canadian Journal of Civil Engineering, 45(10), 878–888.
18. Yi, S.-T. (2022). Analytical Study on Concrete Cover Thickness of Anisotropic FRP Bar. Journal of the Korea institute for structural maintenance and inspection, 26(1), 58–66.

19. Saleem, H. & Elzaroug, O., (2023), Finite element modeling for simulating thermal cracking in GFRP-reinforced concrete slabs, The 1st international conference on civil engineering applications (ISCCEA 2023).
20. Hughes Brothers, Inc. (2002). Aslan 100 Fiber glass Rebars. [Online].Technical Report Data. Available from World Wide Web: <http://www.hughesbros.com
21. Tokyo Sokki Kenkyujo Co., Ltd. (TLM). TML Strain Gauge Users Guide (TML PAM E-101P). Tokyo. http://www.tokyosokki.co.jp/e/.